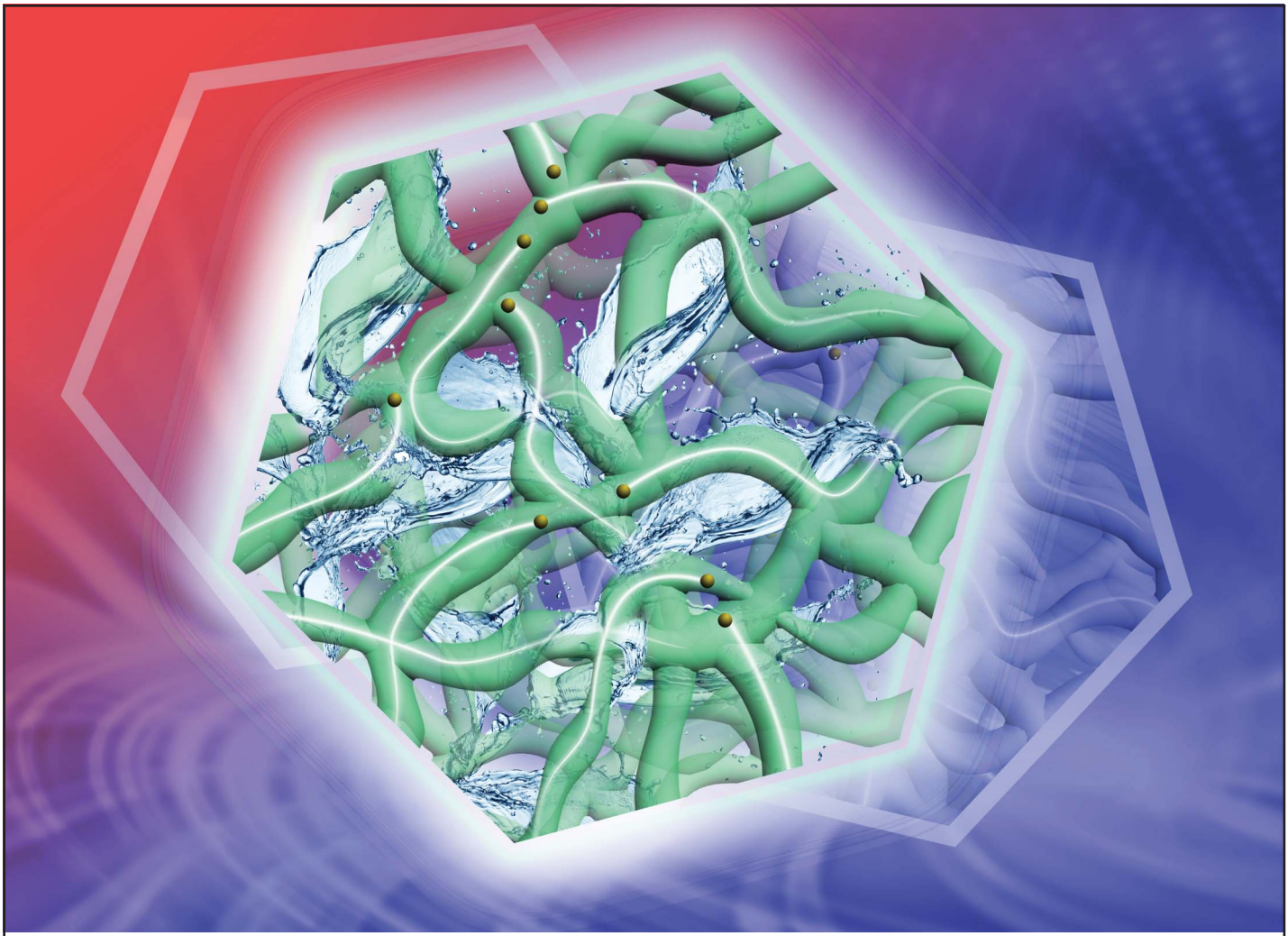

Showcasing the research efforts from Dr. Changzhou Yuan's group at Anhui Key Laboratory of Metal Materials and Processing, School of Materials Science and Engineering, Anhui University of Technology, Ma'anshan, P.R. China.

Title: Polymer-assisted synthesis of a 3D hierarchical porous network-like spinel $NiCo_2O_4$ framework towards high-performance electrochemical capacitors

An intriguing interconnected hierarchical porous 3D network-like $NiCo_2O_4$ architecture is efficiently designed and fabricated *via* a facile yet scaled-up strategy, and yields remarkable specific capacitance and excellent electrochemical stability at high rates for advanced next-generation electrochemical capacitors.

As featured in:

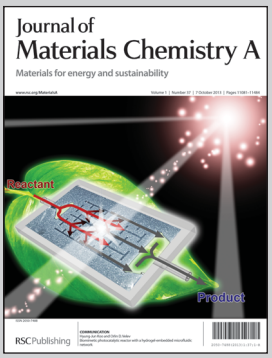

See C. Yuan *et al.*,
J. Mater. Chem. A, 2013, **1**, 11145.

RSC Publishing

www.rsc.org/MaterialsA

Registered Charity Number 207890

Journal of Materials Chemistry A

RSC Publishing

PAPER

View Article Online
View Journal | View Issue

Cite this: *J. Mater. Chem. A*, 2013, **1**, 11145

Polymer-assisted synthesis of a 3D hierarchical porous network-like spinel $NiCo_2O_4$ framework towards high-performance electrochemical capacitors†

Changzhou Yuan,*[ad] Jiaoyang Li,[a] Linrui Hou,[a] Jingdong Lin,*[b] Xiaogang Zhang*[c] and Shenglin Xiong[d]

Received 17th May 2013
Accepted 1st July 2013

DOI: 10.1039/c3ta11949a

www.rsc.org/MaterialsA

We have developed a facile yet scalable polymer-assisted chemical solution route to prepare a three-dimensional (3D) hierarchical porous network-like $NiCo_2O_4$ framework for advanced electrochemical capacitors (ECs). The unique interconnected hierarchical porous framework is constructed by nanosized spinel $NiCo_2O_4$ building blocks of 20–30 nm size, thus, a 3D continuous electron transport expressway, convenient electrolyte penetration–diffusion and large electrode–electrolyte interface are obtained simultaneously. The combination of these appealing structural features in the striking network-like $NiCo_2O_4$ framework results in a drastically enhanced kinetic behavior, large specific capacitance (SC) and a remarkable cycling stability at high rates. The unique network-like $NiCo_2O_4$ electrode features a SC of 587 F g^{-1} at 2 A g^{-1}, and can deliver up to 518 F g^{-1} at a large current density of 16 A g^{-1}. Also, a SC deterioration of ~6% of the maximum SC is evident after continuous 3500 charge–discharge cycles at varying current densities, ranging from 2 to 16 A g^{-1}. Furthermore, the synthetic strategy presented here can be easily extended to fabricate other binary complex metal oxides and/or ternary metal oxides with a controlled composition and porous structure, which may be promising candidates for high-performance ECs, and even advanced Li-ion batteries.

Introduction

Electrochemical capacitors (ECs), as a new class of energy storage device, are now attracting substantial attention owing to their excellent ability to provide energy density higher by orders of magnitude than dielectric capacitors, and a greater power density and longer cycling ability than other conventional rechargeable batteries.[1,2] Significant research interests are thus triggered in the design and development of novel advanced electrode materials for ECs. Particularly, some transition metal oxides (TMOs), such as amorphous RuO_2 and IrO_2, exhibit remarkable electrochemical performances as pseudocapacitive electrode materials, due to their higher specific capacitance (SC) than carbon-based materials and better cycling behavior than conductive polymers.[3–6] Note that an ultrahigh SC value of 1580 F g^{-1} was reported for the state-of-the-art hydrated RuO_2.[3] Nevertheless, it still suffers from the disadvantages of high cost and a toxic nature, excluding it from wide application, which greatly motivates the exploration and screening of alternative economic TMO candidates (such as, MnO_2, NiO, Co_3O_4, V_2O_5, *etc.*)[7–14] with desirable electrochemical behaviors for next-generation ECs. Unfortunately, the intrinsic low electronic conductivities of these simple TMOs with band gaps ranging from 3 to 4 eV[15–17] cannot guarantee their striking electrochemical performance, particularly at high rates.

Recently, an intriguing binary complex TMO, spinel nickel cobaltite ($NiCo_2O_4$), where the Ni species occupies octahedral sites and the Co is distributed over both octahedral and tetrahedral sites (Fig. 1a), came into worldwide view for EC

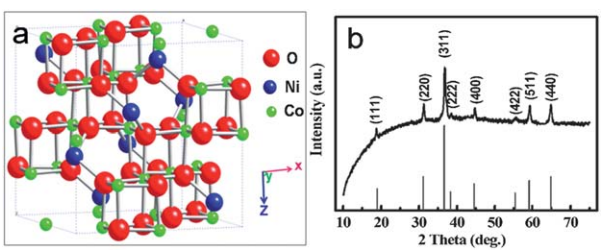

Fig. 1 Crystallographic structure (a) and XRD pattern (b) of the as-synthesized hierarchical porous network-like $NiCo_2O_4$.

[a]*School of Materials Science and Engineering, Anhui University of Technology, Ma'anshan, 243002, P. R. China. E-mail: ayuancz@163.com*

[b]*Department of Chemistry, College of Chemistry and Chemical Engineering, Xiamen University, Xiamen, 361005, P. R. China. E-mail: jdlin@xmu.edu.cn*

[c]*College of Material Science & Engineering, Nanjing University of Aeronautics and Astronautics, Nanjing, 210016, P. R. China. E-mail: azhangxg@163.com*

[d]*Key Laboratory of Colloid and Interface Chemistry (Shandong University), Ministry of Education, P. R. China*

† Electronic supplementary information (ESI) available: Supporting figures. See DOI: 10.1039/c3ta11949a

applications,[18–26] due to its better electrical conductivity, at least two orders of magnitude higher, and a better electroactivity than single nickel oxides or cobalt oxides. It was documented to have 62 S cm^{-1} for the single crystal $NiCo_2O_4$ nanoplate at room temperature,[27] and 0.6 S cm^{-1} for a polycrystalline film at 300 °C.[28] Besides the exceptional feature, other merits, including low cost, abundant resources, environmental friendliness and rich redox reactions, originating from both nickel and cobalt ions,[18–26] render its promising EC application as a scalable alternative pseudocapacitive electrode. Due to its typical Faradaic pseudocapacitive nature involving redox reactions at the electrode–electrolyte interface, it is of significant importance to improve the surface-dependent processes of the $NiCo_2O_4$ electrode with the aim to further optimize its overall energy storage at high rates by rationally designing and tailoring its microstructure.

In general, nanoscaling greatly increases structural interfaces, leading to an enhanced charge transfer, and drastically shortening the ion/electron diffusion pathways by decreasing the grain size and increasing the porosity of the bulk material,[29,30] which may manifest a fascinating electrochemical performance of the electroactive $NiCo_2O_4$. Recently, tremendous attention has been devoted to the synthesis and evaluation of hierarchical porous nanomaterials, for they can integrate morphological features,[15–29] such as a high specific surface area (SSA), rich porosity and good conductivity. However, some repugnant disadvantages still cannot be overlooked including serious aggregation, significant interfacial resistance between adjacent particles even with mesoporosity, and so on,[3,5] resulting in great SC losses and a poor calendar life. To address these issues, an interesting and explored avenue is to efficiently construct a three-dimensional (3D) interconnected hierarchical porous network-like framework composed of nanosized building blocks. Thus, a continuous electron transport path, convenient electrolyte penetration–diffusion and large electrode–electrolyte interface would be simultaneously delivered, which is of great importance for its application in advanced ECs.[30] Additionally, the broad and successful industrial applications of desirable $NiCo_2O_4$ electrodes are greatly limited due to complicated processing routes and expensive fabrication. Therefore, for commercial applications, a facile, scalable and low-cost synthetic procedure is preferable for its mass fabrication.

In this work, we developed a scalable bottom-up synthesis of a 3D hierarchical porous network-like $NiCo_2O_4$ framework through a facile, yet efficient polymer-assisted chemical solution strategy.[31,32] Due to the synergetic effect of ethylenediaminetetraacetic acid (EDTA) and polyethyleneimine (PEI), a unique hierarchical porous network-like architecture derived from interconnected nanoscale spinel $NiCo_2O_4$ building blocks was successfully constructed. Benefitting from these admirable structural features, the hierarchical porous network-like $NiCo_2O_4$ electrode exhibits large SCs, an excellent rate capability and striking cycling stability at high rates, which suggests its great promising applications in ECs.

Experimental section

Synthesis of 3D hierarchical porous network-like $NiCo_2O_4$ framework

A precursor solution was prepared by dissolving 2 mM of $Co(NO_3)_2 \cdot 6H_2O$ and 1 mM of $Ni(NO_3)_2 \cdot 6H_2O$ in 30 mL of deionized H_2O, and then 1 g of ethylenediaminetetraacetic acid (EDTA) and polyethyleneimine (PEI) were added to the solution, under stirring. Then, the mixture was heated on a hot plate to remove excess water in air, and then transferred to a crucible and heated with a heating ramp of 1 °C min^{-1} to a temperature of 500 °C for 1 h. Finally, a black loose foam-like powder was obtained after cooling down to room temperature (RT). For comparison purposes, other $NiCo_2O_4$ samples were also synthesized in a similar fashion, either with the absence of PEI or EDTA, and denoted as $NiCo_2O_4$–EDTA and $NiCo_2O_4$–PEI, respectively.

Materials characterization

The samples were examined by powder X-ray diffraction (XRD) (Max 18 XCE, Japan) using a Cu Ka source ($\lambda = 0.154056$ nm) at a scanning speed of 3° min^{-1} over a 2θ range of 10–75°. The morphologies and structures were observed with field-emission scanning electron microscopy (FESEM, JEOL-6300F, 15 kV) and transmission electron microscopy (TEM), high-resolution transmission electron microscopy (HRTEM), and selected area electron diffraction (SAED) (JEOL JEM 2100 system operating at 200 kV). X-ray photoelectron spectra (XPS) measurements were performed on a VGESCALAB MKII X-ray photoelectron spectrometer with a Mg Ka excitation source (1253.6 eV). Energy dispersive X-ray analysis (EDXA) was performed on FESEM instrument (JEOL-6300F). N_2 adsorption–desorption was determined by the Brunauer–Emmett–Teller (BET) measurement by using an ASAP-2010 surface area analyzer.

Electrochemical tests

The working electrode was prepared with the electroactive material $NiCo_2O_4$, acetylene black and polytetrafluoroethylene in a weight ratio of 8 : 1.5 : 0.5. A small amount of water was then added to make a more homogeneous mixture, which was pressed on to a nickel foam with a surface area of 1 cm^2 ($\sim 10^7$ Pa) for the following electrochemical tests, by cyclic voltammetry (CV), chronopotentiometry (CP) and electrochemical impedance spectroscopy (EIS) measurements performed with a Ivium electrochemical workstation (the Netherlands). The typical loading of the electroactive $NiCo_2O_4$ was 5 mg cm^{-2}. All the experiments were carried out in a three-electrode cell with a working electrode, a platinum plate counter electrode (1 cm^2) and a saturated calomel electrode (SCE) reference electrode at RT. The electrolyte was a 3 M KOH aqueous solution. The cycling performance was carried out with a CT2001D tester (Wuhan, China). The SCs of the $NiCo_2O_4$ electrodes were calculated by using the following equation:

$$C_s = \frac{It}{\Delta V} \quad (1)$$

where C_s is the SC (F g^{-1}) of the $NiCo_2O_4$ electrodes, I donates the discharge current (A g^{-1}), t is the discharging time (s), and ΔV is the discharge potential interval (V).

The time constant (τ) was calculated by using the expression:[33]

$$\tau = \frac{1}{2\pi f^*} \quad (2)$$

where f is the frequency corresponding to the maximum of the imaginary component ($-Z''$) of the semicircle. The EIS "small-signal" capacitance of the $NiCo_2O_4$ electrode can be calculated from the imaginary component of the impedance by using the equation:[34]

$$C = \frac{1}{-2\pi f\, Z'' m} \quad (3)$$

where C is the EIS signal capacitance, f is the frequency (0.01 Hz), m is the mass of the electroactive material, and Z'' is the imaginary component of impedance at the frequency (f = 0.01 Hz). In addition, an important parameter, the coulombic efficiency (η) of the electrodes, can be evaluated from the following equation:

$$\eta = \frac{t_D}{t_C} \times 100\% \quad (4)$$

where t_D and t_C are the time for the galvanostatic discharging and charging, respectively.

Results and discussion

Herein, we applied a typical polymer-assisted chemical solution approach to prepare the 3D hierarchical porous network-like $NiCo_2O_4$ framework by using water soluble polymers, where EDTA and PEI are used to bind with Co^{2+} and Ni^{2+} ions. Specifically, the metal Co and Ni ions in the solution bind with EDTA to form the metal–EDTA complex, which further binds with PEI to form a homogeneous stable solution.[31,32] This ensures a homogeneous metal distribution in the precursor and leads to the final formation of the desired $NiCo_2O_4$ phase with stoichiometry, after calcination in air. The typical X-ray diffraction (XRD) pattern of the as-synthesized $NiCo_2O_4$ sample is shown in Fig. 1b. Evidently, eight well-defined diffraction peaks are observed at 2θ values of 18.9°, 31.1°, 36.7°, 38.3°, 44.6°, 55.4°, 59.1° and 64.9°. All of these peaks, not only including their peak positions but also intensities, can be successfully indexed to the (111), (220), (311), (222), (400), (422), (511) and (440) plane reflections of the spinel $NiCo_2O_4$ crystalline structure (JCPDF file no. 20-0781; space group: F^*3 (202)), respectively, as seen from the standard spectra indicated by the gray lines in Fig. 1b. A calculation using the Debye–Scherrer equation for the broadening of the (311) peak gives an average size of ~27 nm for the as-prepared $NiCo_2O_4$. Of particular note, no other impurities can be detected in the typical pattern, which confirms that the temperature of 500 °C applied here is high enough for the complete thermal conversion of its precursor into pure spinel $NiCo_2O_4$.

To reveal more a detailed elemental make-up and the oxidation state of the as-obtained $NiCo_2O_4$, an X-ray photoelectron spectrum (XPS) was obtained, and the corresponding XPS data is shown in Fig. 2. The Ni 2p spectrum (Fig. 2a) was carefully fitted considering two spin-orbit doublets and two shake-up satellites (donated as "S"). Accordingly, two kinds of nickel species are detected and assigned to the Ni(II) and Ni(III) ions. In specific, the fitted peaks, at a binding energy (BE) of 850.6 and 870.2 eV are ascribed to the Ni(II), whereas the peaks at a BE of 852.5 and 871.9 eV are both assigned to the Ni(III). Furthermore, the fitting results of the Co 2p XPS spectrum are also shown in Fig. 2b. Clearly, two kinds of Co species also can be found, including the Co(III) ions sitting at a BE of 776.3 and 791.7 eV, and Co(II) ions at a BE of 778.3 and 792.6 eV. Note that the Co/Ni ratio is ~2 in the sample, very close to the designed ratio. The high-resolution spectrum for the O 1s region is presented in Fig. 2c. The two oxygen contributions designed as O1 and O2, are evident in Fig. 2c. Specifically, the well-resolved O1 sitting at 531.8 eV corresponds to a higher number of defect sites with a low oxygen coordination in the $NiCo_2O_4$ species with the small size.[35] Meanwhile the fitted peak of O2 at 529.5 eV is typical of a metal-oxygen bond.[36,37] The XPS data clearly demonstrates that the surface of the as-prepared $NiCo_2O_4$ sample has a complex composition containing Co^{2+}, Co^{3+}, Ni^{2+} and Ni^{3+}. Thus, the formula of the obtained $NiCo_2O_4$ can be generally expressed as follows: $Co_{1-x}^{2+}Co_x^{3+}[Co^{3+}Ni_x^{2+}Ni_{1-x}^{3+}]O_4$ ($0 < x < 1$) (the cations within the brackets are in octahedral sites and those outside the brackets are in tetrahedral sites).[38,39] It is due to the presence of the mixed valencies of the same cation in such a cobaltite spinel system that the network-like $NiCo_2O_4$ framework possesses a relatively high electrical conductivity by electron transfer taking place with a relatively low activation energy between the cations by hopping processes.[25]

The representative field-emission scanning electron microscopy (FESEM) images (Fig. 3a and b) of the as-obtained $NiCo_2O_4$ powder show an intimately interconnected network-like

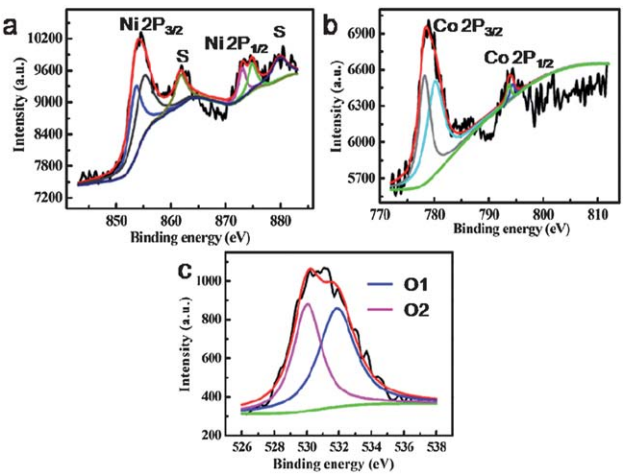

Fig. 2 High-resolution XPS spectra of Ni 2p (a), Co 2p (b) and O 1s (c) for the hierarchical porous network-like $NiCo_2O_4$ sample.

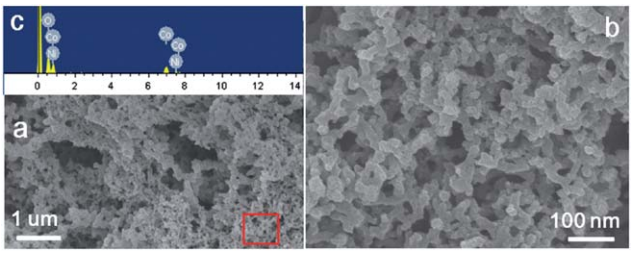

Fig. 3 FESEM images (a and b) and EDXA (c) of the hierarchical porous network-like $NiCo_2O_4$ sample. The image in (b) is taken from the region marked by the rectangle in (a).

structure. Many inter-particle pores can be clearly observed. In addition, the energy dispersive X-ray analysis (EDXA) data (Fig. 3c) also presents the co-existence of the Co and Ni elements with the molar ratio of ~2 : 1, which is very close to that in the precursor solution. The low- and high-magnification transmission electron micrograph (TEM) images (Fig. 4a–c) further confirm the hierarchical meso- and/or macroporous nature of the $NiCo_2O_4$ material and the high degree of pore connectivity in the unique network-like $NiCo_2O_4$ framework. The size of the $NiCo_2O_4$ nano building blocks is 20–30 nm, as evident in Fig. 4c. The selected-area electron diffraction (SAED) pattern (the inset in Fig. 4c), detected from a sampling area indicated by the red rectangle in Fig. 4c, shows well-defined diffraction rings, revealing its polycrystalline characteristics. The high-resolution TEM (HRTEM, Fig. 4d) image shows that some of the nanoparticles (NPs) with different orientations overlap each other, confirming the formation of the interconnected network-like scaffold. Interestingly, the as-prepared hierarchical porous network-like framework cannot be destroyed and broken into discrete individual $NiCo_2O_4$ NPs, even after subjecting it to a lengthy ultrasonication, which suggests that the unique architecture is not a random aggregation of $NiCo_2O_4$ nano building blocks, but an intimated interconnection of these nanodomains.

The N_2 adsorption–desorption isotherm (Fig. S1, ESI†) of the $NiCo_2O_4$ sample shows a sharp capillary condensation step at a high relative pressure, and belongs to a type IV isotherm according to the IUPAC classification,[40] greatly supporting the presence of a typical hierarchical porosity, *i.e.*, meso- and/or macropores in the sample.[41–43] Moreover, a Brunauer–Emmett–Teller (BET) SSA of the unique hierarchical porous $NiCo_2O_4$ framework is estimated as ~40 $m^2\ g^{-1}$. To better understand the formation mechanism, other control experiments were elaborately performed. In sharp contrast, when the precursor solution had no PEI or EDTA, only some simple particle aggregations were found (Fig. S2 and S3, ESI†). According to the results of this analysis, it is easy to conclude that the EDTA and PEI might potentially serve as the initial network in the preparation process,[33] thus efficiently preventing the aggregation of the formed NPs and constructing a 3D interconnected hierarchical porous network-like framework; that is, it is owing to the synergetic effect of the EDTA and PEI that the unique interconnected porous network-like spinel $NiCo_2O_4$ architecture is well constructed. Unquestionably, the continuous hierarchical porous networks of the $NiCo_2O_4$ sample with a desirable electronic conductivity have huge potential applications in high-performance ECs.

Next, we applied the 3D continuous hierarchical porous network-like $NiCo_2O_4$ framework as a pseudocapacitive electrode to highlight the merits of the unique architecture for advanced ECs application. The cyclic voltammetry (CV) was measured at various scan rates ranging from 5 to 70 mV s^{-1} with a three-electrode system in a 3.0 M KOH aqueous solution, and the corresponding CV curves in a potential range of 0.0–0.5 V (*vs.* SCE) are shown in Fig. 5a. The typical CV plots at all scan rates show a pair of well-defined redox peaks, indicating that the capacitive characteristics are mainly governed by the Faradaic redox reactions originating from the M–O/M–O–OH, where the M represents both the Ni and Co ions.[18–26] Also, as the scan rate increases, the current subsequently increases while the CV shape changes little, revealing its good electrochemical capacitance. Notedly, both the electrochemical cathodic and anodic peak currents vary linearly with the sweep rates, as seen from Fig. 5b. This demonstrates that the hierarchical porous network-like $NiCo_2O_4$ electrode has an excellent power property, and the typical capacitive behavior is not diffusion controlled.[44,45]

In order to further confirm the unique electrochemical process for a rapid Faradaic energy storage, electrochemical

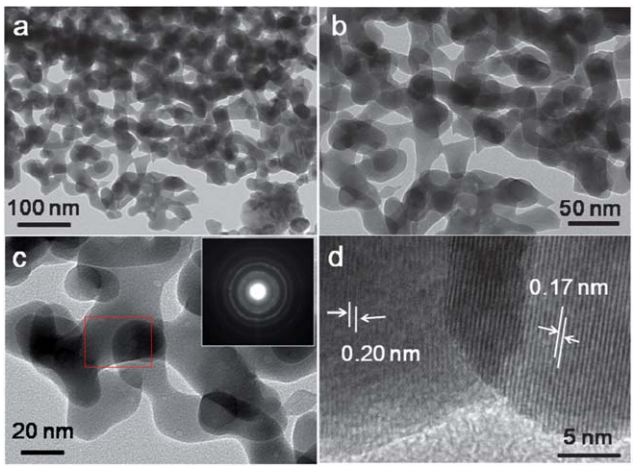

Fig. 4 TEM (a–c), HRTEM (d) images and SAED pattern (the inset in c) of the hierarchical porous network-like $NiCo_2O_4$ framework.

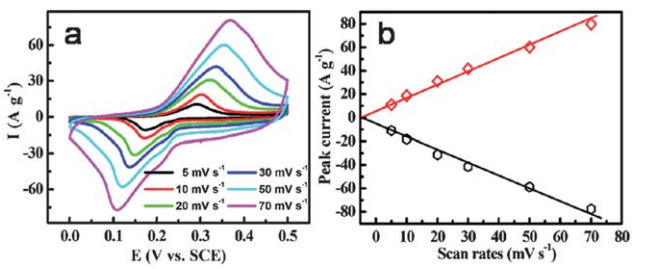

Fig. 5 CV curves at various sweep rates (a) and the relationship between peak current (i_p) and the sweep rate (b) of the hierarchical porous network-like $NiCo_2O_4$ framework electrode.

impedance spectroscopic (EIS) analysis of the hierarchical porous network-like $NiCo_2O_4$ electrode was conducted at the potential of 0.35 V (*vs.* SCE) in the frequency range 0.01–10^5 Hz with an AC signal amplitude of 5 mV. The obtained Nyquist plot typically ($-Z''$ *vs.* Z') is given in Fig. 6. The intersection of the plots at the *x*-axis represents the solution resistance (R_s),[46,47] which is associated with the following three items: the resistance of the KOH aqueous solution, the intrinsic resistance of the electroactive material itself, and the contact resistance at the interface between the electroactive material and the current collector. As seen from the inset, R_s can be found to be only ~0.33 Ω, which suggests the good electronic conductivity of the hierarchical porous network-like $NiCo_2O_4$ electrode itself. In contrast, other $NiCo_2O_4$ electrodes synthesized in the absence of PEI or EDTA demonstrate even higher R_s values of ~0.7 and 0.82 ohm, respectively (Fig. S4, ESI†), which should be related to the increased interfacial resistance between adjacent particles and the larger size. At the high–medium frequency region, a typical semicircle, whose diameter stands for the charge transfer resistance (R_{ct}) in the electrochemical process can be found. The R_{ct} is approximated to ~0.44 Ω, which is much less than those of the $NiCo_2O_4$–PEI (~1.8 ohm) and $NiCo_2O_4$–EDTA (~1.5 ohm) electrodes (Fig. S4, ESI†). Such low values mean the low R_s and R_{ct} of the hierarchical porous network-like $NiCo_2O_4$ electrode during the redox process creates an efficient energy storage. Moreover, from the frequency (147 Hz) corresponding to the maximum of the imaginary component of the semicircle, the time constant (τ), a parameter indicating the power property of an electrode material,[48] can be calculated as ~1 ms. Such a small time constant, of the order of ms, is preferred for its rapid charge–discharge characteristics. The knee frequency of ~3.2 Hz further suggests that the electrode material possesses a good frequency response. Additionally, the Warburg tail expected to occur with a 45° inclination is not seen in the intermediate frequency region, which indicates that the electrolyte ions can access the electroactive material easily, and dominate the fast electrochemical response observed in the CV plots shown in Fig. 5a. While for the other two $NiCo_2O_4$ electrodes synthesized in the absence of PEI or EDTA, an obvious Warburg process with an ion diffusion resistance can be found (Fig. S4, ESI†), for which the two electrodes with a simple particle aggregation, rather than an interconnected continuous network-like architecture, should be responsible. As is evident in Fig. 6, the slope of the impedance plot tends to an almost vertical asymptote along the realistic impedance axis in the low-frequency region less than the knee frequency, characteristic of the admirable capacitative behavior of the unique network-like $NiCo_2O_4$ electrode in the KOH aqueous solution. Accordingly, the EIS "small-signal" capacitance[49] of the unique $NiCo_2O_4$ electrode can be calculated as 468 F g^{-1} ($f = 0.01$ Hz) from the imaginary component of the EIS data.

To further qualify the SCs of the unique hierarchical porous network-like $NiCo_2O_4$ architecture electrode, a chronopotentiometry (CP) test at various mass-normalized current densities ranging from 2 to 16 A g^{-1} was carried out with a maximum electrochemical window of 0.45 V (*vs.* SCE), and the typical discharge curves are depicted in Fig. 7a. Evidently, the nonlinear charge–discharge curves demonstrate that typical Faradaic redox reactions occur at the electrode–electrolyte interfaces, verifying its typical pseudocapacitive characteristic, which is in good agreement with the CV curves (Fig. 5a). The SCs of the hierarchical porous network-like $NiCo_2O_4$ electrode were calculated and are recorded in Fig. 7b. Attractively, the unique electrode exhibits excellent pseudocapacitances of 587, 569, 560, 545 and 518 F g^{-1} at the current densities of 2, 4, 6, 10 and 16 A g^{-1}, respectively, which suggests that ~88% of the capacitance is still maintained when the charge–discharge rate is increased from 2 to 16 A g^{-1}. In sharp contrast, the SC retentions of the $NiCo_2O_4$–PEI and $NiCo_2O_4$–EDTA electrodes only retain as ~68% (from 216 to 320 F g^{-1}) and ~61% (from 158 to 260 F g^{-1}) (Fig. S5, ESI†), respectively, when the current density is up to 16 A g^{-1} from 2 A g^{-1}. The calculation of the pure electric double-layer capacitance (EDLC) by using the BET SSA of an average value of 20 μF cm^{-2} (ref. 50) further delivers an EDLC of ~8 F g^{-1} for the unique hierarchical porous network-like electrode, much lower than the corresponding measured SCs, which ranged from 518 to 587 F g^{-1}. Therefore, it is further demonstrated that the main component of the measured SC is produced from the pseudocapacitive surface redox process, and the Faradaic pseudocapacitance is ~510 F g^{-1}, *i.e.*, 1275 μF cm^{-2} at a large current density of 16 A g^{-1}, revealing a high electrochemical utilization of the network-like $NiCo_2O_4$ electrode at high rates.

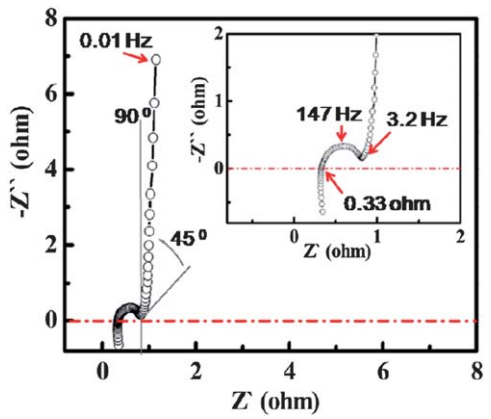

Fig. 6 EIS spectrum of the hierarchical porous network-like $NiCo_2O_4$ electrode measured at 0.35 V (*vs.* SCE). The inset is the enlarged high-frequency region of the EIS spectrum.

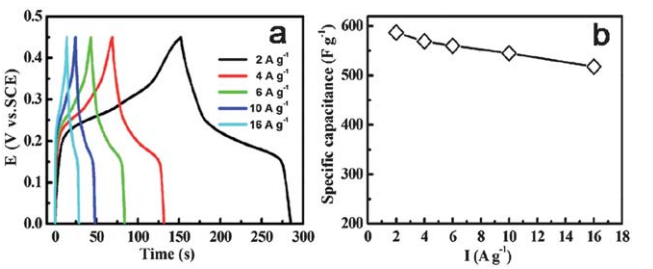

Fig. 7 Charge–discharge curves (E *vs.* time) (a) and calculated SC (b) of the hierarchical porous network-like $NiCo_2O_4$ electrode at different current densities.

These data strongly support the fact that the hierarchical porous network-like $NiCo_2O_4$ framework is an appealing electrode for advanced ECs due to its prominent ability to deliver large SCs and a high electrochemical utilization at a high charge–discharge rate, which might be attributed to the attractive structural features of the present electrode. Specifically, the 3D hierarchical porous network-like feature (Fig. 8) is constructed by interconnected nanosized $NiCo_2O_4$ building blocks, and many interpenetrated meso- and/or macropores are formed, which then reduce the penetration–diffusion length of the electrolyte ions and interfacial resistance, and guarantees that enough electrolyte ions rapidly make contact with the large naked surfaces of the electroactive $NiCo_2O_4$ with the 3D interconnected electron conductive network. More importantly, these inherent interpenetrated meso- and/or macropores can offer a robust sustentation of the OH^- ions, and ensure that sufficient Faradaic reactions take place at high current densities for energy storage, due to its great role of "ion-buffering reservoirs".[33,42,49] This in turn would ensure its good electrochemical utilization and high-rate charge–discharge performance.

All in all, the convenient ionic diffusion path, narrow diameters of the building blocks and continuous electron transfer network can reduce the ionic diffusion resistance and charge transfer resistance, and therefore, the unique hierarchical porous network-like $NiCo_2O_4$ electrode achieves a high electrochemical utilization even at large current densities. Fig. 9 shows the cycling performance of the hierarchical porous network-like $NiCo_2O_4$ electrode at progressively increased current densities in the 3 M KOH aqueous solution. Clearly, the unique network-like $NiCo_2O_4$ electrode exhibits a stable cycling behavior at each current density. The curves show that the SC increases gradually during the first 550 cycles at 2 A g^{-1}, due to a gradual activation process of the electroactive $NiCo_2O_4$,[51,52] and then a maximum SC of 630 F g^{-1} is observed. After another 2200 continuous cycles at larger current densities, of up to 16 A g^{-1}, the current density is turned back to 2 A g^{-1} again. Under this condition, ~98% of the maximum SC at 2 A g^{-1} still can be recovered, and maintains for another 750 cycles with a further SC decrease of ~4%. Moreover, the coulombic efficiency of the unique porous network-like $NiCo_2O_4$ electrode is maintained at more than 89% during the continuous charge–discharge cycles. The electrochemical data recorded in Fig. 9 further highlight the capability of the hierarchical porous network-like $NiCo_2O_4$ electrode to meet the requirements of an excellent electrochemical stability during the long-term cycling under a high-power density operation, which is a significant merit for practical EC devices.

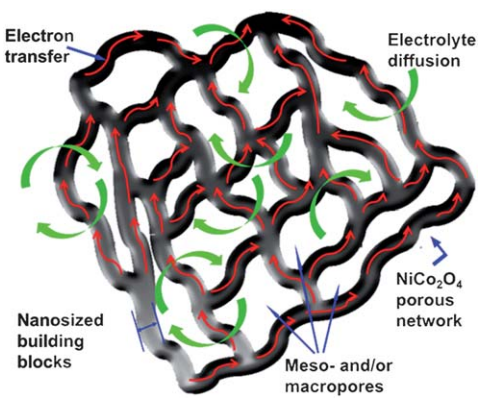

Fig. 8 Schematic illustration of the charge storage advantages of the 3D interconnected hierarchical porous network-like $NiCo_2O_4$ framework electrode.

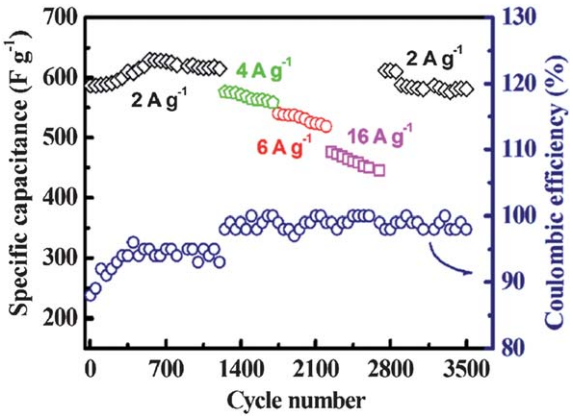

Fig. 9 Cycling performance and coulombic efficiency of the hierarchical porous network-like $NiCo_2O_4$ electrode at progressively varying current densities.

Conclusions

In summary, we have successfully developed a simple cost-effective and scale-up polymer-assisted chemical solution synthesis of a 3D interconnected hierarchical porous network-like $NiCo_2O_4$ framework electrode. The continuous hierarchical porous network creates convenient channels for better ion transport to the redox-active material, and the high degree of pore connectivity in the hierarchical porous network enhances electron transfer, avoids serious particle aggregation, and decreases the great interfacial resistance. Thanks to these advantageous structural benefits, the unique hierarchical porous network-like $NiCo_2O_4$ electrode possessed large SCs and a striking cycling stability at large current densities. The excellent supercapacitive performance encourages its aspired commercial exploitation for the development of advanced ECs. More significantly, we envision that the electrode design concept can be easily generalized to the synthesis of other binary complex metal oxides, and even ternary metal oxides as high-performance electrodes for next-generation ECs, and even advanced Li-ion batteries applications.

Acknowledgements

This work is partly supported by the National Natural Science Foundation of China (no. 51202004 and 21173120), the Nature Science Foundation of Anhui Province (no. KJ2013A051), the Specialized Research Fund for the Doctoral Program of Higher Education of China (no. 20060287026), the Nature Science Foundation of Jiangsu Province (no. BK2011030) and the Foundation of Key Laboratory of Colloid and Interface Chemistry (Shandong University), Ministry of Education (no. 201201).

Notes and references

1 P. Simon and Y. Gogotsi, *Nat. Mater.*, 2008, **7**, 845.
2 B. E. Conway, *Electrochemical Supercapacitors: Scientific Fundamentals and Technological Applications*, Kluwer Academic/Plenum Publishers, New York, 1999.
3 C. C. Hu, W. C. Chen and K. H. Chang, *J. Electrochem. Soc.*, 2004, **151**, A281.
4 M. Hughes, G. Z. Chen, M. S. P. Shaffer, D. J. Fray and A. H. Windle, *Chem. Mater.*, 2002, **14**, 1610.
5 C. Z. Yuan, L. Chen, B. Gao, L. H. Su and X. G. Zhang, *J. Mater. Chem.*, 2009, **19**, 246.
6 W. Sugimoto, H. Iwata, Y. Yasunaga, Y. Murakami and Y. Takasu, *Angew. Chem., Int. Ed.*, 2003, **42**, 4092.
7 O. Ghodbane, F. Ataherian, N. L. Wu and F. Favier, *J. Power Sources*, 2012, **206**, 454.
8 C. Z. Yuan, L. R. Hou, L. Yang, D. K. Li, L. F. Shen, F. Zhang and X. G. Zhang, *J. Mater. Chem.*, 2011, **21**, 16035.
9 B. Saravanakumar, K. K. Purushothaman and G. Muralidharan, *ACS Appl. Mater. Interfaces*, 2012, **4**, 4484.
10 B. Wang, J. S. Chen, Z. Y. Wang, S. Madhavi and X. W. Lou, *Adv. Energy Mater.*, 2012, **2**, 1188.
11 C. Z. Yuan, L. Yang, L. R. Hou, J. Y. Li, Y. X. Sun, X. G. Zhang, L. F. Shen, X. J. Lu, S. L. Xiong and X. W. Lou, *Adv. Funct. Mater.*, 2012, **22**, 2560.
12 M. Hasan, M. Jamal and K. M. Razeeb, *Electrochim. Acta*, 2012, **60**, 193.
13 C. Z. Yuan, L. Yang, L. R. Hou, L. F. Shen, X. G. Zhang and X. W. Lou, *Energy Environ. Sci.*, 2012, **5**, 7883.
14 S. W. Lee, J. Kim, S. Chen, P. T. Hammond and S. H. Yang, *ACS Nano*, 2010, **4**, 3889.
15 F. M. Courtel, H. Duncan, Y. Abu-lebdeh and I. J. Davidson, *J. Mater. Chem.*, 2011, **21**, 10206.
16 V. I. Anisimov, M. A. Korotin and E. Z. Kurmaev, *J. Phys.: Condens. Matter*, 1990, **2**, 3973.
17 V. S. Bagotzky, N. A. Shumilova and E. I. Khrushcheva, *Electrochim. Acta*, 1976, **21**, 919.
18 H. Jiang, J. Ma and C. Z. Li, *Chem. Commun.*, 2012, **48**, 4465.
19 C. Z. Yuan, J. Y. Li, L. R. Hou, X. G. Zhang, L. F. Shen and X. W. Lou, *Adv. Funct. Mater.*, 2012, **22**, 4592.
20 H. L. Wang, Q. M. Gao and L. Jiang, *Small*, 2011, **7**, 2454.
21 T. Wu, J. Y. Li, L. R. Hou, C. Z. Yuan, L. Yang and X. G. Zhang, *Electrochim. Acta*, 2012, **81**, 172.
22 T. Y. Wei, C. H. Chen, H. C. Chien, S. Y. Lu and C. C. Hu, *Adv. Mater.*, 2010, **22**, 347.
23 C. Z. Yuan, J. Y. Li, L. R. Hou, L. Yang, L. F. Shen and X. G. Zhang, *J. Mater. Chem.*, 2012, **22**, 16084.
24 H. W. Wang, Z. A. Hu, Y. Q. Chang, Y. L. Chen, H. Y. Wu, Z. Y. Zhang and Y. Y. Yang, *J. Mater. Chem.*, 2011, **21**, 10504.
25 M. Hamdani, R. N. Singh and P. Chartier, *Int. J. Electrochem. Sci.*, 2010, **5**, 556.
26 C. Z. Yuan, H. B. Wu, Y. Xie and X. W. Lou, *Angew. Chem., Int. Ed.*, 2013, DOI: 10.1002/anie.201303971.
27 L. F. Hu, L. M. Wu, M. Y. Liao, X. H. Hu and X. S. Fang, *Adv. Funct. Mater.*, 2012, **22**, 998.
28 M. R. Tarasevich and B. N. Efremov, in *Electrodes of Conductive Metallic Oxides Part A*, ed. S. Trasatti, Elsevier, USA, 1982, p. 227.
29 J. M. Feckl, K. Fominykh, M. Döblinger, D. Fattakhova-Rohlfing and T. Bein, *Angew. Chem.*, 2012, **124**, 7577.
30 C. Z. Yuan, B. Gao, L. F. Shen, S. D. Yang, L. Hao, X. J. Lu, F. Zhang, L. J. Zhang and X. G. Zhang, *Nanoscale*, 2011, **3**, 529.
31 Q. L. Lin, Y. Xu, E. G. Fu, S. Baber, Z. B. Bao, L. Yu, S. G. Deng, J. Kundu, J. Hollingsworth, E. Bauer, T. M. McCleskey, A. K. Burrell, Q. X. Jia and H. M. Luo, *J. Mater. Chem.*, 2012, **22**, 5835.
32 Q. X. Jia, T. M. Mccleskey, A. K. Burrell, Y. Lin, G. E. Collis, H. Wang, A. D. Q. Li and S. R. Foltyn, *Nat. Mater.*, 2004, **3**, 529.
33 L. R. Hou, C. Z. Yuan, L. Yang, L. F. Shen, F. Zhang and X. G. Zhang, *RSC Adv.*, 2011, **1**, 1521.
34 Y. K. Zhou, B. L. He, W. J. Zhou, J. Huang, X. H. Li, B. Wu and H. L. Li, *Electrochim. Acta*, 2004, **49**, 257.
35 V. M. Jimenez, A. Fernandez, J. P. Espinos and A. R. Gonzalez-Elipe, *J. Electron Spectrosc. Relat. Phenom.*, 1995, **71**, 61.
36 T. Choudhury, S. O. Saied, J. L. Sullivan and A. M. Abbot, *J. Phys. D: Appl. Phys.*, 1989, **22**, 1185.
37 J. F. Marco, J. R. Gancedo and M. Gracia, *J. Solid State Chem.*, 2000, **153**, 74.
38 J. G. Kim, D. L. Pugmire, D. Battaglia and M. A. Langell, *Appl. Surf. Sci.*, 2000, **165**, 70.
39 J. H. Zhong, A. L. Wang, G. R. Li, J. W. Wang, Y. N. Ou and Y. X. Tong, *J. Mater. Chem.*, 2012, **22**, 5656.
40 W. Xiong, M. Liu, L. Gan, Y. Lv, Y. Li, L. Yang, Z. Xu, Z. Hao, H. Liu and L. Chen, *J. Power Sources*, 2011, **196**, 10461.
41 J. R. Matos, M. Kruk, L. P. Mercuri, M. Jaroniec, L. Zhao, T. Kamiyama, O. Terasaki, T. J. Pinnavaia and Y. Liu, *J. Am. Chem. Soc.*, 2003, **125**, 821.
42 C. Z. Yuan, X. G. Zhang, L. H. Su, B. Gao and L. F. Shen, *J. Mater. Chem.*, 2009, **19**, 5772.
43 D. Grosso, G. Illia, E. L. Crepaldi, B. Charleux and C. Sanchez, *Adv. Funct. Mater.*, 2003, **13**, 37.
44 T. Brezesinski, J. Wang, S. H. Tolbert and B. Dunn, *Nat. Mater.*, 2010, **9**, 146.
45 A. J. Bard and L. R. Faulkner, *Electrochemical Methods Fundamentals and Applications*, John Wiley, Inc., New York, 2nd edn, 2001, ch. 6, pp. 233–235.
46 C. Z. Yuan, X. G. Zhang, Q. F. Wu and B. Gao, *Solid State Ionics*, 2006, **177**, 1237.
47 A. Chu and P. Braatz, *J. Power Sources*, 2002, **112**, 236.
48 L. Cao, M. Lu and H. L. Li, *J. Electrochem. Soc.*, 2005, **152**, A871.
49 D. W. Wang, F. Li, M. Liu, G. Q. Lu and H. M. Cheng, *Angew. Chem., Int. Ed.*, 2008, **47**, 373.
50 Y. T. Wu and C. C. Hu, *J. Electrochem. Soc.*, 2004, **151**, A2060.
51 C. C. Hu, K. H. Chang and T. Y. Hsu, *J. Electrochem. Soc.*, 2008, **155**, F196.
52 C. H. Wang, X. Zhang, D. C. Zhang, C. Yao and Y. W. Ma, *Electrochim. Acta*, 2012, **63**, 220.